

# Investigation of a Cross-Slot-Coupled Dual-Band Circularly Polarized Hybrid Dielectric Resonator Antenna

Meng Zou\*, Jin Pan, Le Zuo, and Zai-Ping Nie

**Abstract**—In this paper, a cross-slot-coupled dual-band circularly polarized (CP) hybrid dielectric resonator antenna (DRA) is presented. The design concept is based on using a cross-slot as both a feeding structure of the DRA and an effective radiator. Full wave simulation is used to verify the proposed design concept in this paper. A prototype antenna is designed, fabricated, and measured. Good agreement is obtained between the simulated and measured results.

## 1. INTRODUCTION

The dielectric resonator antenna (DRA) [1, 2] has a number of inherent advantages, such as small size, wide bandwidth, and low loss. These features make DRA an attractive candidate for many applications. With the development of wireless communication systems, DRAs with dual-band performance have been widely investigated [3–5]. Hybrid DRA [6–12] technology is a viable candidate for realizing dual-band operation. A direct approach to designing a hybrid DRA is to introduce an extra slot resonator [9]. However, this method will lead to a complicated antenna configuration. A simpler approach to designing a hybrid DRA is to take advantage of the resonance of the feeding structure. In [10], a compact wideband DRA was obtained by merging the resonances of the slot coupled DRA and the DR loaded slot. In [11], an ultra-wideband hybrid antenna was proposed by combining the annular DRA with a monopole that simultaneously acts as a feed structure and a radiator. And a dual-band hybrid DRA fed by a coplanar waveguide has been reported in [12].

In those studies, the hybrid DRAs are designed based on the first order approximation model [14], that is, the resonances of the dielectric resonator (DR) and the feeding structure are independent. For example, in [10] the dielectric waveguide model (DWM) method [13] is used to calculate the resonant frequency of the DR, and an approximate formula for computing effective permittivity is used to estimate the resonant frequency of the slot. In reality, the DR is placed on a ground plane with a coupling slot, which is not considered in the DWM. The introduction of the coupling slot will influence the resonance of the DR, but it has not been discussed. Moreover, the effects of the cross-sectional dimensions of DR and substrate on the resonance of the slot are not included in the approximate formula for effective permittivity.

As we know, antennas with circular polarization (CP) [15–25] can reduce polarization mismatch between transmitting and receiving antennas in wireless communication systems. However, most of the previous work on the hybrid DRAs, which makes use of the resonance of the feeding structure, was primarily concentrated on linearly polarized designs. And only a few such antennas with dual-band CP performance have been reported. In [15], a wideband CP hybrid DRA coupled by four sequentially rotated slots was proposed. A quite complex feeding network is employed in this design in order to realize 90° phase difference among the four slots. Dual-band circularly polarized hybrid DRA can also

---

*Received 8 August 2014, Accepted 25 September 2014, Scheduled 1 October 2014*

\* Corresponding author: Meng Zou (zm.1598@163.com).

The authors are with the Department of Microwave Engineering, School of Electronic Engineering, University of Electronic Science and Technology of China, Chengdu 611731, P. R. China.

be obtained by combining DRA with a zonal slot antenna [23, 24]. However, the sizes of the hybrid CP DRAs in [23, 24] are large because of the introductions of the conducting cavity.

In this paper, effects of coupling slot on the resonances of the DR and effects of the cross-sectional dimensions of the DR on resonances of the cross-slot are studied. Based on the discussion, a cross-slot-coupled dual-band CP DRA is presented by using the concept of hybrid DRA. The cross-slot can be regarded as both a feeding structure of the DRA and a ceramic-loaded cross-slot antenna. A dual-band CP antenna can be obtained when the dimensions of the cross-slot are properly chosen. The hybrid operation of the proposed DRA is demonstrated. Several key parameters and their effects on the performances of the proposed antenna are studied, and the results are presented and discussed.

## 2. DESIGN CONCEPT

The geometry of the proposed cross-slot-coupled dual-band CP hybrid DRA is shown in Figure 1. The structure of the proposed antenna is very simple. It is made up of two parts: a rectangular DR and a microstrip line fed cross-slot fabricated on the substrate. The DRA has dimensions of  $a \times b \times c$ , and dielectric constant of  $\epsilon_r$ . The width of the cross-slot is  $w$ , and the arm lengths of the cross-slot are  $l_2 = l$  and  $l_1 = l + \Delta l$ . The slot arm with length of  $l_1$  is named as arm 1, and the slot arm with length of  $l_2$  is named as arm 2. The grounded substrate has dimensions of  $l_g \times l_g \times t$  and dielectric constant of  $\epsilon_s$ . For achieving a good impedance matching at both bands, the fed line consists of a  $50 \Omega$  microstrip line, which has a length of  $l_{m1}$  and a width of  $w_{m1}$ , and an impedance transformer with  $l_{m2}$  and  $w_{m2}$ .

The proposed antenna is designed as a hybrid CP antenna. It can be regarded as the combination of a cross-slot-coupled DRA and a ceramic-loaded cross-slot antenna. For the cross-slot-coupled DRA, radiating structure is the DR on the ground plane, and feeding structure is the cross-slot. In this design, the lowest two modes in the rectangular DR are excited with a  $90^\circ$  phase difference to realize CP operation. For the ceramic-loaded cross-slot antenna, cross-slot is the radiating structure and the DR acts as a superstrate. The slots resonate at approximately  $\lambda_g/2$ , where  $\lambda_g = \lambda_0/\sqrt{\epsilon_{eff}}$  is the guided wavelength of the equivalent magnetic current in the slot sandwiched between substrate and DR. The effective permittivity  $\epsilon_{eff}$  is estimated by

$$\epsilon_{eff} \approx \frac{\epsilon_s \epsilon_r (t + c)}{(\epsilon_s c + \epsilon_r t)} \quad (1)$$

where  $(\epsilon_s, t)$ ,  $(\epsilon_r, c)$  are the permittivities and heights of the substrate and DR, respectively. In this design, the cross-slot-coupled DRA is for the lower band and the ceramic-loaded cross-slot antenna for the upper band. The proposed antenna is right-hand circularly-polarized (RHCP) at both bands because  $l_1 > l_2$ .

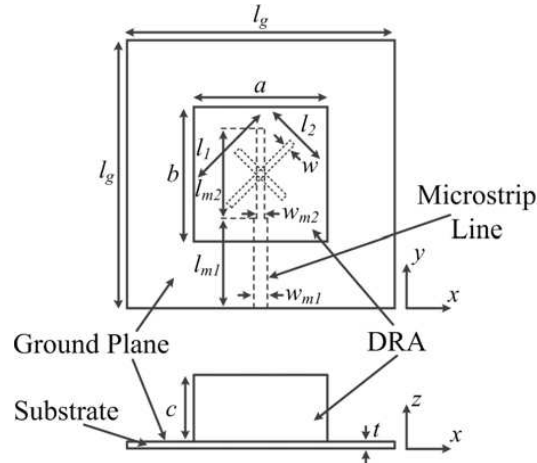


**Figure 1.** Configuration of the cross-slot-coupled dual-band CP hybrid DRA.

The full wave simulator Ansoft HFSS [26] based on finite element method is used to calculate the resonant frequencies and fields of the modes in the DR and cross-slot in this paper. Figure 2(a) and Figure 2(b) show the  $H$ -fields and resonant frequencies of the lowest two modes, respectively, when the cross-slot has dimensions of  $l = 20$  mm,  $\Delta l = 5.5$  mm, and  $w = 1.5$  mm. The  $H$ -fields of the  $TE_{111}^x$  and  $TE_{111}^y$  modes are rotated because of the introduction of the cross-slot on the ground plane.  $H$ -fields of the lowest and second lowest modes are along arm 1 and arm 2, respectively. Therefore, the two modes can be named as  $TE_{111}^{\text{arm1}}$  and  $TE_{111}^{\text{arm2}}$  modes. The lowest two resonant frequencies of the DRA and that of the cross-slot as functions of  $l$ , when  $\Delta l = 5.5$  mm and  $w = 1.5$  mm, are shown in Figure 4(a). The lower resonant frequency of the cross-slot is due to the slot with length of  $l_1$  and the higher one is due to the slot with length of  $l_2$ .  $H$ -fields of the  $TE_{113}$  modes are shown in Figure 3. The cross-slot also has similar effects on the  $TE_{113}$  modes of the DR. The resonant frequencies of the  $TE_{113}^{\text{arm1}}$  and  $TE_{113}^{\text{arm2}}$  modes as functions of  $l$  are shown in Figure 4(b). Based on the data shown in Figure 4, it is convenient to justify a dual-band antenna is a hybrid DRA or a DRA taking advantage of the higher order modes.

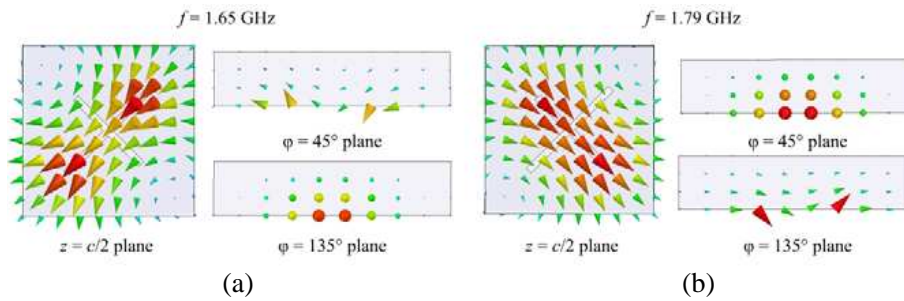


**Figure 2.** Resonant frequencies and  $H$ -fields of the lowest two modes of the DR placed on a ground plane with a cross-slot ( $l = 20$  mm,  $\Delta l = 5.5$  mm, and  $w = 1.5$  mm). (a) The lowest mode. (b) The second lowest mode.

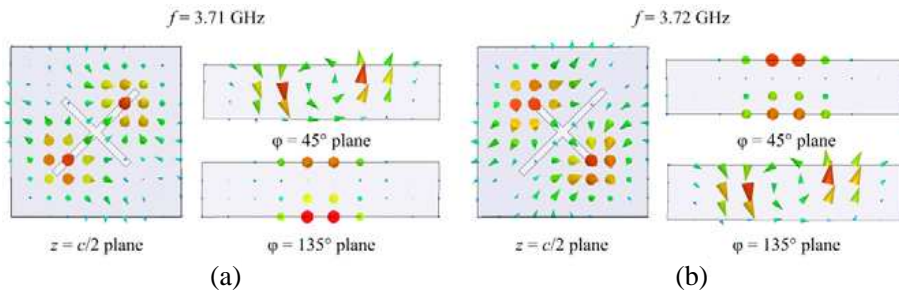


**Figure 3.** Resonant frequencies and  $H$ -fields of the  $TE_{113}$  modes of the DR placed on a ground plane with a cross-slot ( $l = 20$  mm,  $\Delta l = 5.5$  mm, and  $w = 1.5$  mm). (a)  $TE_{113}^{\text{arm1}}$  mode. (b)  $TE_{113}^{\text{arm2}}$  mode.

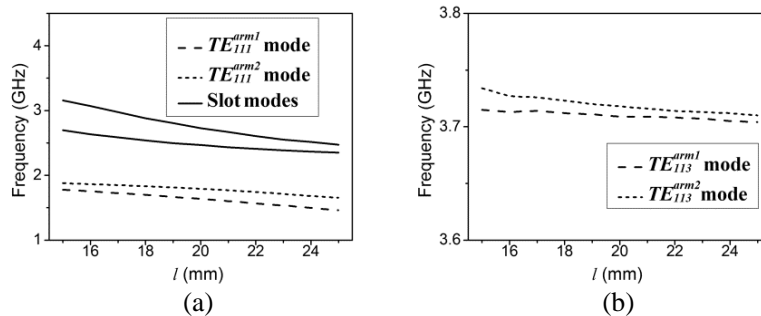


**Figure 4.** Resonant frequencies of the DR and cross-slot as functions of  $l$ . (a)  $TE_{111}^{\text{arm1}}$ ,  $TE_{111}^{\text{arm2}}$ , and slot modes. (b)  $TE_{113}^{\text{arm1}}$  and  $TE_{113}^{\text{arm2}}$  modes.

### 3. PARAMETER ANALYSIS AND DISCUSSION

A prototype antenna with parameters shown in Table 1 was designed by HFSS. The simulated input impedance and return loss are shown in Figure 5. There are four resonances within the frequency band of 1.70–2.90 GHz, which occur at  $f_1 = 1.86$  GHz,  $f_2 = 1.97$  GHz,  $f_3 = 2.53$  GHz and  $f_4 = 2.69$  GHz, respectively. The resonant frequencies of the  $TE_{111}$  and  $TE_{113}$  modes of the DR and the lowest two resonant frequencies of the cross-slot are listed in Table 2 to justify the hybrid operation of the DRA. The resonant frequencies of the  $TE_{111}$  modes and cross-slot are obtained from Figure 4(a) and that of the  $TE_{113}$  modes are obtained from Figure 4(b). From Table 2,  $f_1$  and  $f_2$  corresponding to the  $TE_{111}^{\text{arm1}}$  and  $TE_{111}^{\text{arm2}}$  modes of the DR, respectively, and  $f_3$  and  $f_4$  are due to the resonances of the cross-slot. The resonant frequencies of DRA are not equal to that of the DR and cross-slot because the microstrip feed line has effects on the position of the resonances of the DRA [10]. This provides evidence that the proposed antenna is a dual-band hybrid DRA. The cross-slot-coupled DRA is for the lower band and the ceramic-loaded cross-slot antenna is for the upper band.

In order to investigate the effects of some key parameters on the antenna performances at the two bands, parameter analysis is performed.

**Table 1.** Parameter values of the optimized antenna design.

Parameters	Values	Parameters	Values
$a$	37 mm	$l_g$	75 mm
$b$	37 mm	$t$	1.6 mm
$c$	14 mm	$\epsilon_s$	4.4
$\epsilon_r$	12	$l_{m1}$	18.4 mm
$w$	1.5 mm	$w_{m1}$	3 mm
$l$	19.6 mm	$l_{m2}$	28.2 mm
$\Delta l$	5.5 mm	$w_{m2}$	1 mm

**Table 2.** Simulated resonant frequencies of the six modes.

	$TE_{111}^{\text{arm1}}$ mode	$TE_{111}^{\text{arm2}}$ mode	$TE_{113}^{\text{arm1}}$ mode	$TE_{113}^{\text{arm2}}$ mode	Slot mode 1	Slot mode 2
Resonant frequency (GHz)	1.65	1.80	3.71	3.72	2.48	2.77

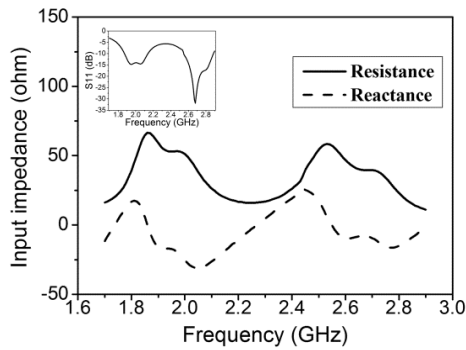


**Figure 5.** Simulated input impedance and return loss.

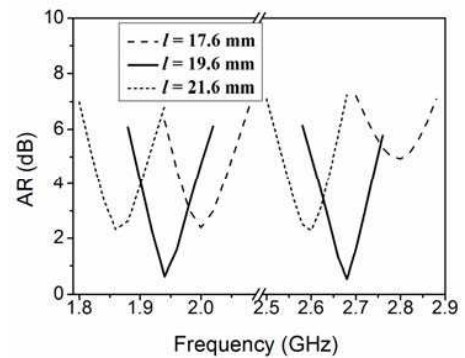


**Figure 6.** Simulated AR for different  $l$ .

Figure 6 shows the simulated AR for different values of  $l$ . From Figure 6, the length  $l$  has a significant impact on the CP performance at both bands. To improve the CP performance of the antennas with  $l = 17.6$  mm and  $l = 21.6$  mm, the values of  $\Delta l$  are optimized, and the results are shown in Figure 7. It can be found that for a fixed value of  $l$ ,  $\Delta l$  can be adjusted to improve the AR in the upper band of the antenna, but good CP performance in the lower band cannot be achieved. Simulated AR for different values of  $w$  is shown in Figure 8.

Figure 9 shows the simulated results of the antenna when  $l_{m2}$  and  $w_{m2}$  are varied. And Figure 10 shows the simulated results of the antenna when  $l_{m1}$  and  $w_{m1}$  are varied. From Figure 9 and Figure 10, good impedance matching can be achieved by optimizing the dimensions of the stepped microstrip line, while it does not harm the AR of the proposed antenna. The dimensions of the feeding line have significant effects on antenna gain. The main reason is that the return loss of the proposed antenna changes along with the dimensions of the feeding line.

Figure 11 shows the effects of cross-slot parameters on antenna gain, when impedance matching is

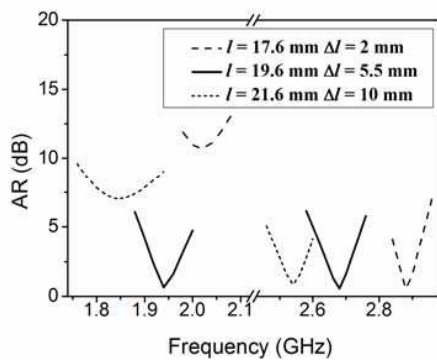


Figure 7. Simulated AR for different  $l$  and  $\Delta l$ .

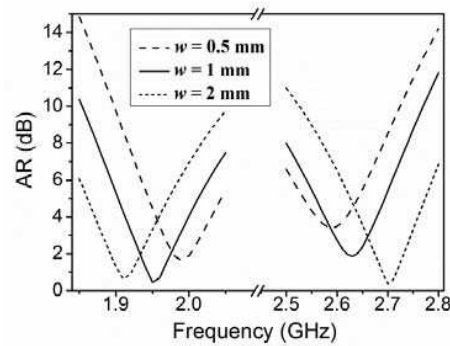
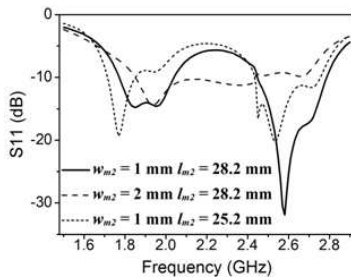
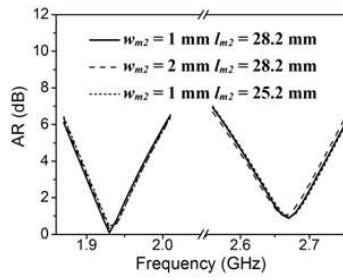


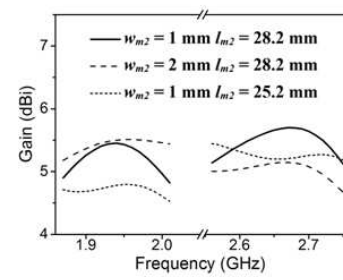
Figure 8. Simulated AR for different  $w$ .



(a)

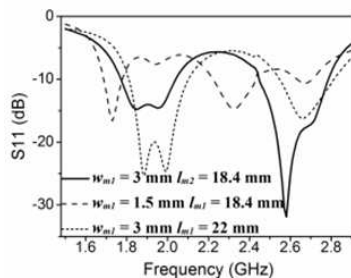


(b)

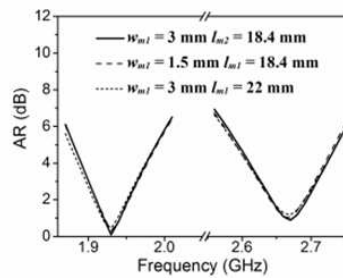


(c)

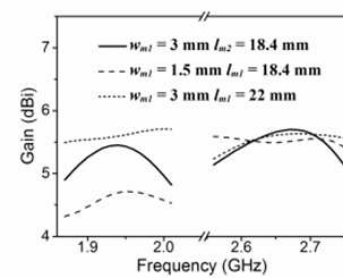
Figure 9. Simulated results for different  $l_{m2}$  and  $w_{m2}$ . (a) Return loss. (b) Axial ratio. (c) Gain.



(a)



(b)



(c)

Figure 10. Simulated results for different  $l_{m1}$  and  $w_{m1}$ . (a) Return loss. (b) Axial ratio. (c) Gain.

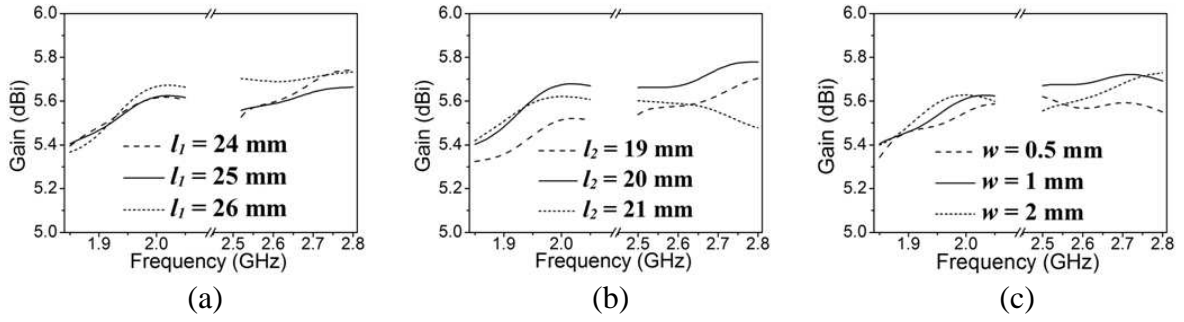


**Figure 11.** The effects of cross-slot parameters on antenna gain. (a) Gain for different  $l_1$ . (b) Gain for different  $l_2$ . (c) Gain for different  $w$ .

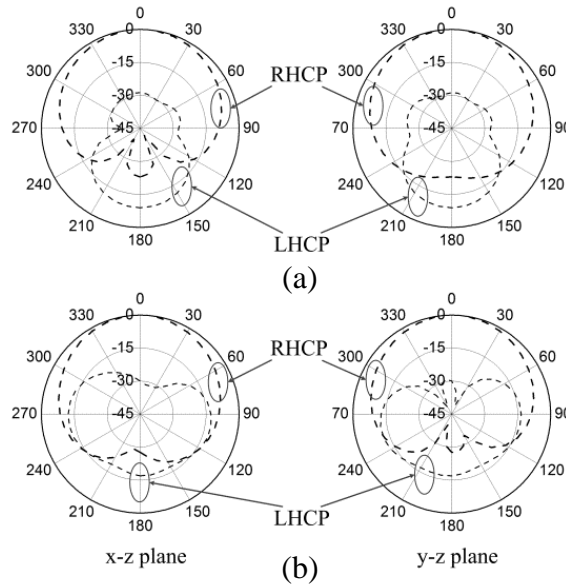


**Figure 12.** Simulated radiation patterns of the cross-slot-coupled dual-band CP hybrid DRA. (a)  $f = 1.94$  GHz. (b)  $f = 2.68$  GHz.

**Table 3.** Effects of ground size  $l_g$  on the front-to-back ratio at the two CP operating frequencies.

Front-to-back ratio (dB)			
	$l_g = 50$ mm	$l_g = 5$ mm	$l_g = 100$ mm
Lower frequency	3.9	8.7	10.6
Upper frequency	16.5	16.5	15.5

achieved at the two bands by tuning the dimensions of the stepped microstrip line. Changing dimensions of the cross-slot will change both field distributions and resonant frequencies of the  $TE_{111}^{\text{arm1}}$ ,  $TE_{111}^{\text{arm2}}$  and slot modes. And that is the reason why the dimensions of cross-slot affect the antenna gain at both the two bands.

The simulated radiation patterns of the proposed antenna at the center frequencies of the two CP bands (1.94 and 2.68 GHz) are shown in Figure 12. As shown in Figure 12, the front-to-back ratio of the proposed antenna at 2.68 GHz is much higher than that at 1.94 GHz. The effects of ground size  $l_g$  on the front-to-back ratio at the two CP operating frequencies are shown in Table 3. When  $l_g$  increases

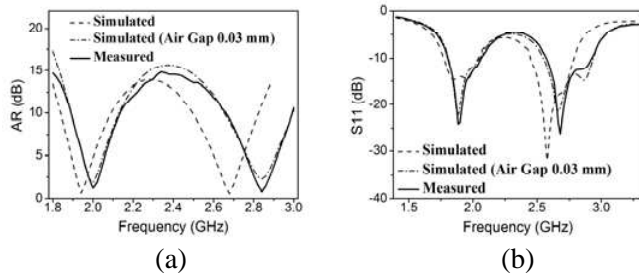
from 50 mm to 100 mm, the front-to-back ratio at the lower frequency increases from 3.9 dB to 10.6 dB (171.8% increase) while that at the upper frequency decreases from 16.5 dB to 15.5 dB (6.1% decrease). The reason why it increases 171.8% at the lower frequency is that the backlobe radiation of a DRA is introduced by the finite ground plane. Thus a big ground plane will lead to a high front-to-back ratio. For a slot antenna, the front-to-back ratio is decided by the materials on the two sides of the slot antenna [27], so it is slightly sensitive to the size of the ground plane.

#### 4. MEASURED RESULTS

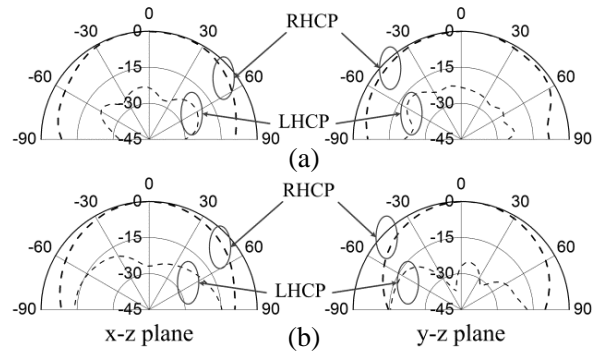
The proposed antenna with parameters shown in Table 1 was fabricated and measured. The measurements were performed using an Agilent vector network analyzer and a SATIMO measurement system.

Figure 13(a) shows the simulated and measured ARs in the boresight direction. The antenna has two operating frequency bands of CP. The measured 3-dB AR bandwidth of the lower band is 3.0% (1.97–2.03 GHz). And the measured 3-dB AR bandwidth of the upper band is 3.5% (2.79–2.89 GHz). As shown in Figure 13(b), the measured impedance bandwidths ( $S_{11} < -10$  dB) are 14.0% (1.80–2.07 GHz) and 12.8% (2.57–2.92 GHz), which cover the lower and upper 3-dB AR bandwidths, respectively. From Figure 13, the measured center frequency of the upper band is higher than the simulated one. This is caused by the air gap [28], which is not existent in the simulations in Section 3, between the DR and the ground plane. The simulated results of the proposed antenna with 0.03 mm air gap are shown in Figure 13. As shown in Figure 13, the measured results agree well with simulated ones when the air gap is 0.03 mm.

The measured radiation patterns of the proposed antenna at 2.00 and 2.84 GHz are shown in Figure 14. The radiation patterns are symmetrical in both  $x$ - $z$  and  $y$ - $z$  planes at 2.00 and 2.84 GHz.



**Figure 13.** Measured and simulated results of the proposed antenna. (a) Axial ratio. (b) Return loss.



**Figure 14.** Measured radiation patterns of the cross-slot-coupled dual-band CP hybrid DRA. (a)  $f = 2.00$  GHz. (b)  $f = 2.84$  GHz.

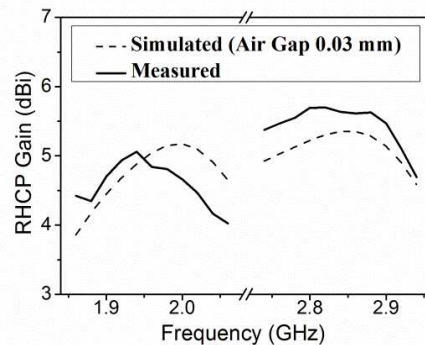


**Figure 15.** Simulated and measured RHCP gain of the cross-slot-coupled dual-band CP hybrid DRA.

**Table 4.** Comparisons between the proposed antenna and other dual-band CP hybrid DRAs. ( $f_0$  is the center frequency of the upper band,  $\lambda_0$  the free-space wavelength at  $f_0$ ,  $H$  the maximum height, and  $L$  the maximum length).

Description	$f_0$ (GHz)	AR BW (lower band)	AR BW (upper band)	Maximum Dimensions
Present DRA	2.84	3.0%	3.5%	$H = 0.15\lambda_0$ , $L = 0.35\lambda_0$
DRA in [23]	5.76	3.5%	4.9%	$H = 0.64\lambda_0$ , $L = 0.60\lambda_0$
DRA in [24]	5.17	3.3%	3.7%	$H = 0.54\lambda_0$ , $L = 0.57\lambda_0$

From Figure 15, the measured RHCP gain of the proposed antenna appears to be 4.7 dBi at 2.00 GHz and 5.6 dBi at 2.84 GHz, respectively.

Comparisons between the proposed antenna and the published dual-band CP hybrid DRAs are given in Table 4. From Table 4, the 3-dB AR bandwidths of the proposed antenna are comparable with that of the antennas reported in [23, 24]. However, the size of the proposed antenna is much more compact than those of the two antennas reported in [23, 24].

## 5. CONCLUSION

In this paper, a cross-slot-coupled dual-band CP hybrid DRA has been proposed. By using the cross-slot as both a feeding structure of the DRA and an effective radiator, a dual-band CP DRA has been obtained. Full wave simulations on the resonant modes of the DR and cross-slot are carried out to justify the hybrid operation of the proposed design. The effects of several key parameters are presented and discussed. Prototype of the proposed antenna has been constructed to certify the validity of the design concept. The discrepancies between the simulated and measured results are explained.

## REFERENCES

1. Long, S. A., M. McAllister, and L. C. Shen, "The resonant cylindrical dielectric cavity antenna," *IEEE Trans. Antennas Propag.*, Vol. 31, No. 3, 406–412, May 1983.
2. Luk, K. M. and K. W. Leung, *Dielectric Resonator Antennas*, Research Studies Press, Hertfordshire, UK, 2003.
3. Chang, T.-H. and J.-F. Kiang, "Dualband split dielectric resonator antenna," *IEEE Trans. Antennas Propag.*, Vol. 55, No. 11, 3155–3162, Nov. 2007.
4. Pan, Y. M., S. Y. Zheng, and B. J. Hu, "Design of dual-band omnidirectional cylindrical dielectric resonator antenna," *IEEE Antennas Wireless Propag. Lett.*, Vol. 13, 710–713, 2014.
5. Almpanis, G., C. Fumeaux, and R. Vahldieck, "Dual-mode bridge-shaped dielectric resonator antennas," *IEEE Antennas Wireless Propag. Lett.*, Vol. 9, 103–106, 2010.
6. Gao, Y., B.-L. Ooi, and A. P. Popov, "Dual-band hybrid dielectric resonator antenna with CPW-fed slot," *Microwave Opt. Technol. Lett.* Vol. 48, No. 1, 170–172, Jan. 2006.
7. Chen, H.-M., Y.-K. Wang, Y.-F. Lin, S.-C. Lin, and S.-C. Pan, "A compact dual-band dielectric resonator antenna using a parasitic slot," *IEEE Antennas Wireless Propag. Lett.*, Vol. 8, 173–176, 2009.
8. Ding, Y. and K. W. Leung, "On the dual-band DRA-slot hybrid antenna," *IEEE Trans. Antennas Propag.*, Vol. 57, No. 3, 624–630, Mar. 2009.
9. Denidni, T. A. and Q. Rao, "Hybrid dielectric resonator antennas with radiating slot for dual-frequency operation," *IEEE Antennas Wireless Propag. Lett.*, Vol. 3, 321–323, 2004.
10. Buerkle, A., K. Sarabandi, and H. Mosallaei, "Compact slot and dielectric resonator antenna with dual-resonance, broadband characteristics," *IEEE Trans. Antennas Propag.*, Vol. 53, No. 3, 1020–1027, Mar. 2005.

11. Lapiere, M., Y. M. M. Antar, A. Ittipiboon, and A. Petosa, "Ultra wideband monopole/dielectric resonator antenna," *IEEE Microw. Wireless Compon. Lett.*, Vol. 15, No. 1, 7–9, Jan. 2005.
12. Lin, Y. F., H. M. Chen, and C. H. Lin, "Compact dual-band hybrid dielectric resonator antenna with radiating slot," *IEEE Antennas Wireless Propag. Lett.*, Vol. 8, 6–9, 2009.
13. Mongia, R. K. and A. Ittipiboon, "Theoretical and experimental investigations on rectangular dielectric resonator antennas," *IEEE Trans. Antennas Propag.*, Vol. 45, No. 9, 1348–1356, Sep. 1997.
14. Kajfez, D. and P. Guillon, *Dielectric Resonators*, Noble, Atlanta, GA, 1998.
15. Massie, G., M. Caillet, M. Clenet, and Y. M. M. Antar, "A new wideband circularly polarized hybrid dielectric resonator antenna," *IEEE Antennas Wireless Propag. Lett.*, Vol. 9, 347–350, 2010.
16. Huang, C.-Y., J.-Y. Wu, and K.-L. Wong, "Cross-slot-coupled microstrip antenna and dielectric resonator antenna for circular polarization," *IEEE Trans. Antennas Propag.*, Vol. 47, No. 4, 605–609, Apr. 1999.
17. Almpanis, G., C. Fumeaux, and R. Vahldieck, "Offset cross-slot-coupled dielectric resonator antenna for circular polarization," *IEEE Microw. Wireless Compon. Lett.*, Vol. 16, No. 8, 461–463, Aug. 2006.
18. Zou, M., J. Pan, Z. Nie, and P. Li, "A wideband circularly polarized rectangular dielectric resonator antenna excited by a lumped resistively loaded monofilar-spiral-slot," *IEEE Antennas Wireless Propag. Lett.*, Vol. 12, 1646–1649, 2013.
19. Chair, R., S. L. S. Yang, A. A. Kishk, K. F. Lee, and K. M. Luk, "Aperture fed wideband circularly polarized rectangular stair shaped dielectric resonator antenna," *IEEE Trans. Antennas Propag.*, Vol. 54, No. 4, 1350–1352, Apr. 2006.
20. Hady, L. K., A. A. Kishk, and D. Kajfez, "Dual-band compact DRA with circular and monopole-like linear polarizations as a concept for GPS and WLAN applications," *IEEE Trans. Antennas Propag.*, Vol. 57, No. 9, 2591–2598, Sep. 2009.
21. Malekabadi, A., M. H. Neshati, and J. Rashed-Mohassel, "Circular polarized dielectric resonator antennas using a single probe feed," *Progress In Electromagnetics Research C*, Vol. 3, 81–94, 2008.
22. Zainud-Deen, S. H., H. A. El-Azem Malhat, and K. H. Awadalla, "A single-feed cylindrical superquadric dielectric resonator antenna for circular polarization," *Progress In Electromagnetics Research*, Vol. 85, 409–424, 2008.
23. Ding, Y., K. W. Leung, and K. M. Luk, "Circularly-polarized DRA-slot hybrid antenna for dualband applications," *Proc. Int. Conf. on Electromag. in Adv. Applicat.*, 880–882, Sep. 2007.
24. Ding, Y., K. W. Leung, and K. M. Luk, "Compact circularly polarized dualband zonal-slot/DRA hybrid antenna without external ground plane," *IEEE Trans. Antennas Propag.*, Vol. 59, No. 6, 2404–2409, Jun. 2011.
25. Malekabadi, S. A., A. R. Attari, and M. M. Mirsalehi, "Compact and broadband circular polarized microstrip antenna with wideband axial-ratio bandwidth," *International Symposium on Telecommunications, IST 2008*, 106–109, Aug. 2008.
26. HFSS Software is Distributed by the Ansoft Corp., Available Online: <http://www.ansoft.com>.
27. Kominami, M., D. M. Pozar, and D. H. Schaubert, "Dipole and slot elements and arrays on semi-infinite substrates," *IEEE Trans. Antennas Propag.*, Vol. 33, No. 6, 600–607, Jun. 1985.
28. Shum, S. M. and K. M. Luk, "Characteristics of dielectric ring resonator antenna with an air gap," *Electron. Lett.*, Vol. 30, No. 4, 277–278, Feb. 1994.